

Using electron vortex beams to determine chirality of crystals in transmission electron microscopy

Roeland Juchtmans,¹ Armand Béch e,¹ Artem Abakumov,¹ Maria Batuk,¹ and Jo Verbeeck¹

¹*EMAT, University of Antwerp, Groenenborgerlaan 171, 2020 Antwerp, Belgium*

We investigate electron vortex beams scattering on chiral crystals. We start by studying point scatterers on a helix, where we derive a relation between the handedness of the helix and the topological charge of the electron vortex on one hand, and the symmetry of the Higher Order Laue Zones in the diffraction pattern on the other. We then extend this to atoms arranged on a helix as found in crystals which belong to chiral space groups and propose a new method to determine the handedness of such crystals within the kinematical approximation. The technique avoids the need for dynamical simulations and makes it possible to determine the handedness of extremely thin samples in which multiple scattering is suppressed. In order to verify the model, elastic scattering simulations are performed and an experimental demonstration on $\text{Mn}_2\text{Sb}_2\text{O}_7$ is given where we find the sample to belong to the right handed variant of the enantiomorphic pair. This technique demonstrates how electron vortex beam diffraction can be used to study chiral materials in transmission electron microscopy.

PACS numbers: 61.05.J-, 03.65.Vf, 41.85.-p

An object is said to be chiral if it is not superposable onto its mirror image by rotating and/or translating it. As such, chiral objects come in two forms, an original and its mirror image called enantiomorphs. In crystals, chirality manifests itself in the crystal's space group (SG). SGs can be divided in three classes, of which the first contains all the SGs having an improper symmetry operation (inversion center, mirror plane, glide plane or roto-inversion axes), which represent non-chiral crystals. Class II includes the 22 SGs which have a screw axis apart from the 2_1 -screw axis. These SGs are chiral and can be divided in 11 enantiomorphic pairs, listed in table (I). Because of the screw axis, atoms in these crystals are arranged in a helical way. The last class contains SGs which possess only proper rotations and/or a 2_1 -screw axis. Crystals belonging to these space groups also are chiral, but when mirrored the space group of the crystal doesn't change, therefore the SG itself is achiral.

1. (P4 ₁ , P4 ₃)	5. (P6 ₁ , P6 ₅)	9. (P3 ₁ , P3 ₂)
2. (P4 ₁ 32, P4 ₃ 32)	6. (P6 ₂ , P6 ₄)	10. (P3 ₁ 12, P3 ₂ 12)
3. (P4 ₁ 22, P4 ₃ 22)	7. (P6 ₁ 22, P6 ₅ 22)	11. (P3 ₁ 21, P3 ₂ 21)
4. (P4 ₁ 2 ₁ 2, P4 ₃ 2 ₁ 2)	8. (P6 ₂ 22, P6 ₄ 22)	

TABLE I. The 22 chiral space groups in class II, divided in 11 enantiomorphic space group pairs.

Determining the chirality of a crystal is of importance when investigating its chiral properties, e.g. optical activity, chiral dichroism and chemical reactions with other chiral molecules. Doing this in a transmission electron microscope, however, appears to be a difficult task. In transmission electron microscopy, the crystal is seen (at least for the so-called zeroth order Laue zone (ZOLZ) in the diffraction pattern) as a two-dimensional projection

through the thickness of the sample. Because of this, one can never distinguish between enantiomorphs since mirroring the crystal along the projection plane changes the handedness of the material, but not its projection on this plane. Therefore, all 3 dimensions have to be taken into account. In a first technique proposed by Goodman et al. [1], this is done by rotating the object and taking several ZOLZ electron diffraction patterns. Another way to gather information on the dimension perpendicular to the projection plane, is to look at so-called Higher Order Laue Zones (HOLZ) in the diffraction pattern [2]. Friedel's law however imposes extra symmetry in the diffraction pattern that does not allow to determine the chirality in kinematical approximation [3]. Therefore multiple scattering (dynamical approximation) is used to break this symmetry and to allow determining the chirality. All methods developed so far thus require dynamical simulations and depend in a sensitive way on sample thickness. An additional difficulty is that not all HOLZ diffraction spots are sensitive to the handedness of the crystal and one has to identify these to be able to determine the chirality of the crystal [4, 5]. In this work, we propose the use of electron vortex beams to break the symmetry imposed by Friedel's law as an alternative way to distinguish SGs in one of the enantiomorphic SG pairs from table (I) without having to rely on dynamical scattering.

As described theoretically by Nye and Berry [6], vortex waves are solutions of the 3D-wave equation with an angular dependent phase factor of the form

$$\Psi(\mathbf{r})_m = \psi(r, z)e^{im\phi}, \quad (1)$$

with r and ϕ the radial and the azimuthal coordinate with respect to the wave propagation axis, z . The number m is referred to as the topological charge. As an eigenstate of the angular momentum operator $L_z = -i\hbar\frac{\partial}{\partial\phi}$, they carry a well-defined angular momentum of $m\hbar$ per electron [7].

In the center of the vortex, the phase is ill-defined and the intensity of the beam becomes zero because of destructive interference, resulting in the typical donut-like intensity profile. Ever since the first experimental realization of optical vortex beams over two decades ago [8], they have been subject to active research which has led to applications varying from nano-manipulation [9–11], astrophysics [12–15] and telecommunication [16–18]. More recently, the first electron vortex beam [19] was created by making a phase plate of stacked graphite layers [20], followed by holographic reconstruction as a more reliable way of producing electron vortices [21]. New ways are still being developed and currently single mode vortex beams at high current as well as atomic size vortices have been realized [22, 23]. Several studies suggest practical use of electron vortex beams in EMCD experiments [21], nano-manipulation [24], spin-polarization devices [25] and magnetic plasmons [26].

Friedel’s law is only applicable to plane wave scattering. Therefore diffraction patterns obtained by vortex beam scattering can be fundamentally different when scattered on enantiomorphic objects, even in the kinematical approximation. The central question in this letter is: “Are electron vortex beams capable of distinguishing chiral crystals within the kinematical approximation?” We will tackle this problem by looking at crystals in chiral space groups in which the atoms are arranged along a helical axis.

In order to understand vortex scattering on helical objects, we consider an infinite string of point scatterers distributed equidistantly on a helix. In Supplemental Material (SM) [27] we derive an analytical expression for the scattering amplitude, $A(\mathbf{k})$, of a vortex beam centered along the helix’ central axis. The probability for the vortex electron to scatter in the direction determined by the wave vector \mathbf{k} is given by $|A(\mathbf{k})|^2$ and gives rise to a diffraction pattern. Within the kinematical approximation, we find for a vortex beam with topological charge m :

$$A_v^m(\mathbf{k}'_{\perp}) \propto \sum_{N=-\infty}^{\infty} (-i)^{NQ} e^{i(m-av+NQ)\phi_k} J_{m-av+NQ}(k'_{\perp}R), \quad (2)$$

where $v = \frac{P}{2\pi}(k_z - k'_z) \in \mathbb{N}$, $k'_{\perp} = \sqrt{k_z^2 - k'_z{}^2}$, P the pitch and R the radius of the helix, Q the number of point scatterers on each pitch and $a = +1$ for a right- and $a = -1$ for a left-handed helix. Note that because of the periodicity in the z -direction, the diffraction pattern consists of discrete rings, which we will label with the number v , corresponding to the ZOLZ ($v = 0$) and HOLZs ($v > 0$) in conventional electron diffraction patterns. From eq. (2) it follows that when m is not a multiple of Q , the HOLZ rings will be different for a left- and right-handed helix. Moreover we find an extra centrosymmetry for rings for which $v = am + nQ$, $n \in \mathbb{Z}$ (see SM [27]), eg. the FOLZ, $v = 1$, will be point symmetric when a right handed vortex, $m = +1$, is

scattered on a right handed helix, $a = +1$.

We apply this model as an approximation of a vortex beam scattered on a helical crystal when the probe is centered on a screw axis and predominantly illuminates a set of heavy atoms distributed on a helix as sketched in fig. (1). The crystal potential in real space can then be approximated by the convolution of the helix potential with the potential of a single heavy atom. In Fourier space, the crystal potential is given by the product of the Fourier transform of the helix and the atom potential. Since the latter is spherically symmetric, the angular dependency of the total Fourier transform stays the same. This means that, if we neglect the phase and intensity variation of the vortex beam over the size of one atom, the intensity profile of each Laue zone will still be given by eq. (2). The only effect caused by the atomic scattering factor is a modulation of the intensity with respect to the scattering angle.

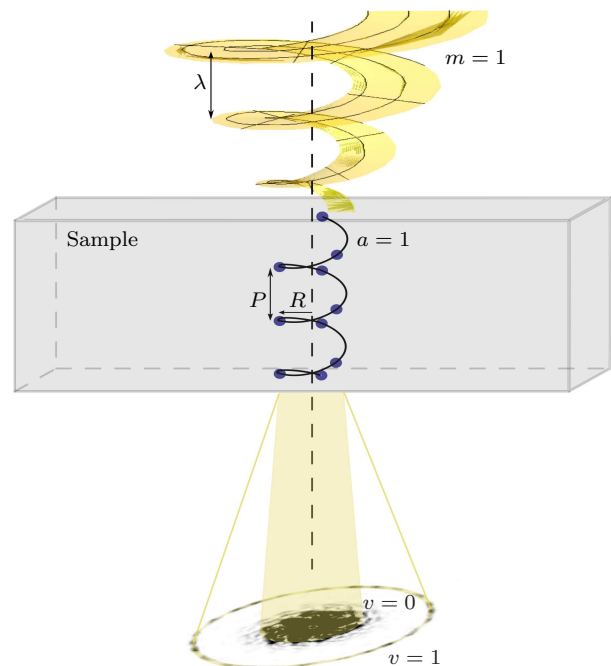


FIG. 1. [Colour online] Schematic representation of the experimental setup. A vortex beam is focused directly on a screw axis in the sample further simplified assuming elastic scattering is dominated by the helically arranged heavy atoms. The radius of the vortex is chosen such that it matches the distance of the atoms to the screw axis.

Eq. (2) shows that we can detect the chirality of a crystal within the kinematical approximation by looking at the HOLZs ($v > 1$) of the diffraction pattern of an electron vortex beam focused on a screw axis in the crystal. For sufficiently thin crystals, the dynamical calculations, which depend strongly on the exact thickness of the sample, can be replaced with a simple comparison of the HOLZs with eq. (2). Moreover, for crystals with a 3-fold screw axis ($Q = 3$), some of the HOLZs will have

an extra centrosymmetry depending on the topological charge of the vortex and the chirality of the crystal, revealing the latter at first glance.

In what follows we will demonstrate our new approach on $\text{Mn}_2\text{Sb}_2\text{O}_7$. From Scott et al. [28] we know this crystal belongs to the space group $P3_121$ or $P3_221$ in which the atoms lie on a right- resp. left-handed 3-fold helix. One of the three inequivalent screw axes only has one heavy *Sb*-atom in its vicinity and electron scattering of a focused (vortex) electron beam centered on this axis approximates the situation of scatterers on a helix. We will determine the chirality of the SG by determining the handedness of this screw axis, which we will refer to without further specification.

In order to verify whether the symmetry predicted in eq. (2) still holds for a vortex beam scattered on a real crystal where other effects occur, e.g. dynamical scattering and spreading of the beam, we perform multislice simulations using the program STEMsim [29]. We look at $\text{Mn}_2\text{Sb}_2\text{O}_7$ along the crystallographic [001] direction, the direction of the screw axis, and focus the vortex beam over it. We choose the semi-convergence angle of the beam such that the radius of the vortex matches the distance of the *Sb*-atoms to the screw axis, i.e. 1.2 Å. For a 300keV vortex beam with $m = \pm 1$ the convergence angle corresponding to this criterion is 8 mrad. The resulting CBED patterns for left- and right-handed vortices scattered on right-handed $\text{Mn}_2\text{Sb}_2\text{O}_7$, thickness 20 nm are given in fig. (2). Here we see that the FOLZ of the left-handed vortex shows only 3-fold symmetry, whereas in the case of the right-handed vortex, the FOLZ shows sixfold symmetry. When scattered on the left-handed enantiomorph, the CBED patterns for vortices with opposite topological charge are swapped, which is consistent with eq. (2).

Next we demonstrate our technique experimentally on a crushed $\text{Mn}_2\text{Sb}_2\text{O}_7$ crystal deposited on a carbon grid. The QuAnTem, a double C_s corrected FEI Titan³ microscope, operating at 300keV, was used. The vortex beams are created with an aperture on which a magnetized needle is mounted, similar to the setup described by B  ch   et al. [22].

After making a high-resolution image of a nano-crystal in the [001] zone-axis, the beam was pointed exactly on top of the screw axis and the diffraction pattern was recorded with a CCD camera (1s exposure time).

We recorded five CBED-patterns using a vortex with topological charge $m \approx +1$ and six patterns with $m \approx -1$ scattered on the same crystal. Because the beam is much smaller than the unit cell size, the symmetry of the diffraction pattern is very sensitive to the position of the probe. Two images recorded with opposite vortices which showed the highest 3-fold symmetry in the diffraction pattern, are compared with the simulated ones in fig. (2). We adjusted the contrast such that only the peaks in the FOLZ are visible and see that the recorded FOLZs qualitatively match the simulations for the right handed crystal rather well.

As it is our intention to determine the chirality of

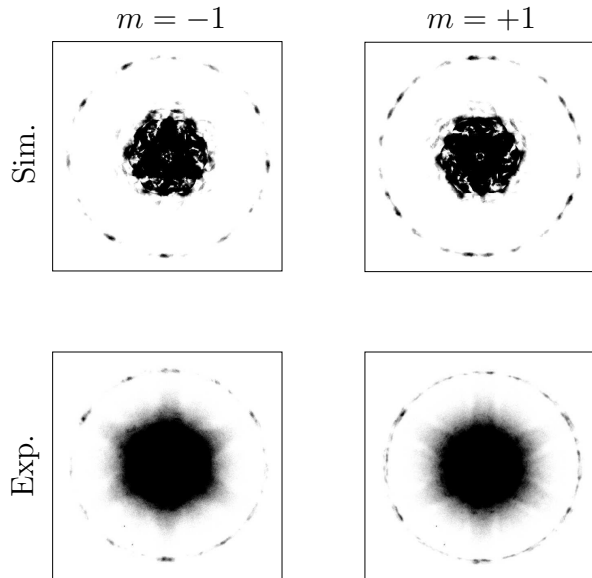


FIG. 2. (Upper) Multislice simulation of first order Laue zone of the diffraction pattern of a $m = -1$ (left) and an $m = +1$ vortex (right) scattered on right handed $\text{Mn}_2\text{Sb}_2\text{O}_7$, with SG $P3_121$. The vortex is centered along the screw axis with the size of the vortex equal to the distance of the *Sb*-atoms from the screw axis, approx. 1.2 Å. The energy of the probe is 300 keV, the convergence angle 8 mrad and the spherical aberration $1 \mu\text{m}$. The thickness of the sample is 20 nm. The centrosymmetry of the first order ring can be seen for the right-handed enantiomorph for $m = +1$. (Lower) Experimental CBED pattern of a 1.2 Å sized vortex probe pointed on a 3-fold screw axis in $\text{Mn}_2\text{Sb}_2\text{O}_7$ for $m = -1$ (left) and $m = +1$ (right). The contrast was adapted to show only the peaks in the FOLZ.

the crystal without comparing the experiment with simulation, we look at the symmetry of the FOLZ ring. To do so in more detail, we plot $I_{FOLZ}(\theta)$, the azimuthal intensity profile of the FOLZ integrated over a small radius ($r, r + dr$), in fig. (3) for the azimuthal coordinate $\theta \in \{0, \pi\}$ (in blue) and for $\theta \in \{\pi, 2\pi\}$ (in red). Although there are some differences between the $(0, \pi)$ and the $(\pi, 2\pi)$ -range for the simulated $m = +1$, the position of the peaks is clearly centrosymmetric, which is not at all the case for the simulated $m = -1$ (see arrows in fig. 3). When looking at the experimental $I_{FOLZ}(\theta)$ it can be seen that most peaks in the $m = +1$ data have a peak at $\theta' = \theta + \pi$. For $m = -1$ we can see peaks in the $(0, \pi)$ -range, which are not present in $(\pi, 2\pi)$ -range, indicating that the FOLZ here is not centrosymmetric. From this we conclude that the crystal under investigation has a right-handed screw axis and thus belongs to $P3_121$.

The major difficulty of this method and the main reason for the deviations of the symmetry in the experiment, is the probe positioning which has to be maintained during the acquisition of the diffraction pattern.

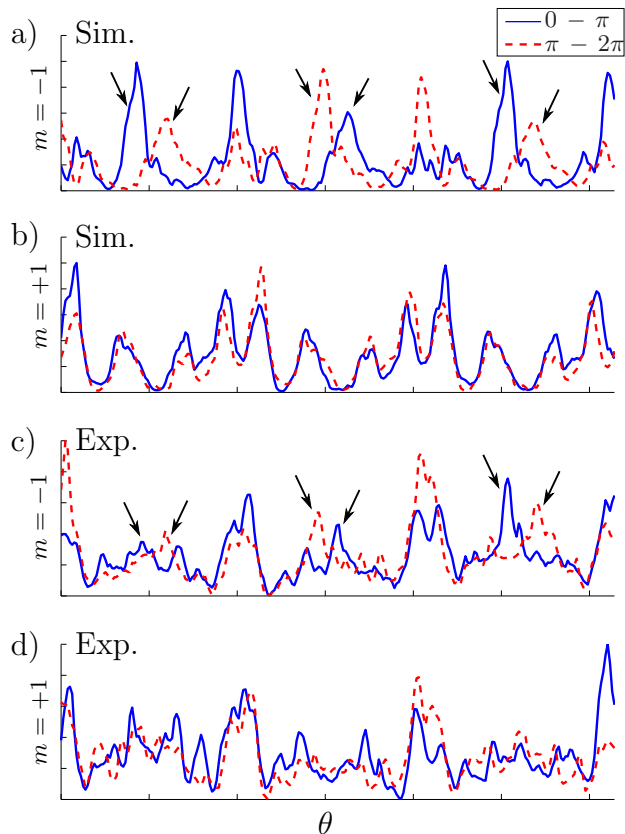


FIG. 3. [Colour online] Comparison of the simulated (a and b) and experimental (c and d) $I_{FOLZ}(\theta)$ for $\theta \in \{0, \pi\}$ (blue) and $\theta \in \{\pi, 2\pi\}$ (red) for $m = -1$ (a and c) and $m = +1$ (b and d). From the position of the peaks it is clear that the $m = +1$ vortex scattered on the right-handed screw axis gives a centrosymmetric FOLZ, which is not the case for the $m = -1$ vortex, where the differences are indicated with arrows.

In conclusion we showed that vortex beam diffraction can be sensitive to the chirality of a crystal, even within the kinematical approximation. As an example, we calculated analytically the scattering amplitude of a vortex scattered on point scatterers arranged on a helix and found that the angular intensity profiles of the HOLZs depend on the topological charge of the vortex and the chirality of the helix. For helices with odd screw axis symmetry it was found that the chirality can be determined unambiguously from the symmetry in the diffraction pattern.

Based on this, we demonstrate a new technique to determine the handedness of a chiral SG by focusing a vortex probe over a screw axis in the crystal. We verified this with multislice simulations on $\text{Mn}_2\text{Sb}_2\text{O}_7$ and give an experimental demonstration of the technique. We used the symmetry property of the FOLZs to determine the handedness of the crystal, thus demonstrating the qualitative character of the technique. The major difficulty is the required accuracy of the probe positioning, which, in combination with sample drift, makes acquisition of the data cumbersome. The 4D-STEM method proposed by Ophus et al. ([30]) might help in overcoming this problem.

The handedness of space groups with a 4-fold or a 6-fold screw axis can be determined in a similar manner, with the exception that one can no longer use the symmetry of the rings, but has to compare $I_{HOLZ}(\theta)$ with eq. (2). Naturally, the use of vortices to determine the chirality of a crystal isn't restricted to crystals with a screw axis with only one heavy atom as nearest neighbor. In general, vortex diffraction is sensitive to the position of atoms in the direction perpendicular to the zone-axis, making them a potentially valuable tool to determine the chirality of crystals, even when they don't belong to one of the chiral SGs in table I.

Although this technique has its experimental challenges, it has the advantage that the chirality of a crystal can be determined within the kinematical approximation such that dynamical calculations can be avoided and that the chirality of very thin samples in which multiple scattering is limited, can be measured. On top of that, this can be done on a local basis, for each position in the crystal, opening the route for probing the chirality of crystals on at near atomic resolution or for investigating screw dislocations in non-chiral crystals. Finally, this work shows the first applications of electron vortex beam diffraction in crystallography where the chiral character of the probe has a significant influence on the diffraction pattern and its symmetry.

The authors acknowledge support from the FWO (Aspirant Fonds Wetenschappelijk Onderzoek - Vlaanderen), the EU under the Seventh Framework Program (FP7) under a contract for an Integrated Infrastructure Initiative, Reference No. 312483-ESTEEM2, and the European Research Council under the FP7 and ERC Starting Grant 278510 VORTEX.

-
- [1] P. Goodman and T. Secomb, *Acta Cryst. A* **33**, 126 (1977).
 - [2] P. Goodman and A. Johnson, *Acta Cryst. A* **33**, 997 (1977).
 - [3] G. Friedel, *C.R. Acad. Sci. Paris* **157**, 1533 (1913).
 - [4] A. Johnson and A. Preston, *Ultramicroscopy* **55**, 348 (1994).
 - [5] H. Inui, A. Fujii, and K. Tanaka, *Acta Cryst. B*, 802 (2003).
 - [6] J. F. Nye and M. V. Berry, *Proc. R. Soc. London A* **336**, 165 (1974).
 - [7] L. Allen, M. W. Beijersbergen, R. J. C. Spreeuw, and J. P. Woerdman, *Phys. Rev. A* **45**, 8185 (1992).
 - [8] V. Bazhenov, M. Vasnetsov, and M. Soskin, *Jetp. Lett.* **52**, 429 (1990).
 - [9] Z.-P. Luo, Y.-L. Sun, and K.-N. An, *Appl. Phys. Lett.* **76**, 1779 (2000).
 - [10] H. He, M. E. J. Friese, N. R. Heck-

- enberg, and H. Rubinsztein-Dunlop, *Phys. Rev. Lett.* **75**, 826 (1995).
- [11] M. E. J. Friese, H. Rubinsztein-Dunlop, J. Gold, P. Hagberg, and D. Hanstorp, *Appl. Phys. Lett.* **78**, 547 (2001).
- [12] G. Foo, D. M. Palacios, and G. a. Swartzlander, *Opt. Lett.* **30**, 3308 (2005).
- [13] G. Swartzlander and R. Hernandez-Aranda, *Phys. Rev. Lett.* **99**, 163901 (2007).
- [14] E. Serabyn, D. Mawet, and R. Burruss, *Nature* **464**, 1018 (2010).
- [15] G. Berkhout and M. Beijersbergen, *Phys. Rev. Lett.* **101**, 100801 (2008).
- [16] D. Andrews, ed., *Structured Light and Its Applications: An Introduction to Phase-Structured Beams and Nanoscale Optical Forces* (Elsevier Science, 2011).
- [17] J. Wang, J.-Y. Yang, I. M. Fazal, N. Ahmed, Y. Yan, H. Huang, Y. Ren, Y. Yue, S. Dolinar, M. Tur, and A. E. Willner, *Nature Phot.* **6**, 488 (2012).
- [18] S. Roychowdhury, V. K. Jaiswal, and R. P. Singh, *Opt. Comm.* **236**, 419 (2004).
- [19] K. Y. Bliokh, Y. P. Bliokh, S. Savel'ev, and F. Nori, *Phys. Rev. Lett.* **99**, 190404 (2007).
- [20] M. Uchida and A. Tonomura, *Nature* **464**, 737 (2010).
- [21] J. Verbeeck, H. Tian, and P. Schattschneider, *Nature* **467**, 301 (2010).
- [22] A. B ech e, R. Van Boxem, G. Van Tendeloo, and J. Verbeeck, *Nature Phys.* **10**, 26 (2014).
- [23] L. Clark, A. B ech e, G. Guzzinati, A. Lubk, M. Mazilu, R. Van Boxem, and J. Verbeeck, *Phys. Rev. Lett.* **111**, 064801 (2013).
- [24] J. Verbeeck, H. Tian, and G. Van Tendeloo, *Adv. Mater.* **25**, 1114 (2013).
- [25] E. Karimi, L. Marrucci, V. Grillo, and E. Santamato, *Phys. Rev. Lett.* **108**, 044801 (2012).
- [26] Z. Mohammadi, C. P. Van Vlack, S. Hughes, J. Bornemann, and R. Gordon, *Opt. Expr.* **20**, 15024 (2012).
- [27] "See supplemental material at [] for derivation and properties of vortex scattering amplitude."
- [28] H. G. Scott, *J. Solid State Chem.* **66**, 171 (1987).
- [29] A. Rosenauer and M. Schowalter, in *Springer Proceedings in Physics (Microscopy of Semiconducting Materials Conference, Cambridge)*, Vol. 120 (2007) p. 169.
- [30] C. Ophus, P. Ercius, C. Sarahan, M. Czarnik, and J. Ciston, *Acta Cryst. A* **70**, C1455 (2014).
- [31] M. D. Graef, *Introduction to Conventional Transmissino Electron Microscopy* (Cambridge University Press, 2003).
- [32] Q. Wang, O. Ronneberger, and H. Burkhardt, *Fourier Analysis in Polar and Spherical Coordinates*, Tech. Rep. 1 (IIF-LMB, Computer Science Department, University of Freiburg, 2008).

Supplemental Material: Using Electron Vortex Beams to distinguish enantiomorphic space groups in a transmission electron microscope

I. VORTEX SCATTERING IN CYLINDRICAL COORDINATES WITHIN THE KINEMATICAL APPROXIMATION

Assuming the scattered part of the wave to be much smaller than the incoming part, the 1st order Born-approximation considers the potential as a small perturbation and describes only single scattering events. Within this approximation the scattering amplitude for an incoming wave $\psi_0(\mathbf{r})$ to scatter on a potential $V(\mathbf{r})$ to a plane wave with wave vector \mathbf{k}' is proportional to [31]

$$A(\mathbf{k}') = \langle \mathbf{k}' | V(\mathbf{r}) | \psi_0 \rangle \propto \int d\mathbf{r} e^{-i\mathbf{k}' \cdot \mathbf{r}} V(\mathbf{r}) \psi_0(\mathbf{r}). \quad (1)$$

Our aim is to find an expression for the vortex beam scattering amplitude. We start from eq. (1) for the scattering amplitude in the Born-approximation of a vortex electron with TC m on a potential $V(\mathbf{r})$:

$$A_m(\mathbf{k}') = \int d\mathbf{r} e^{-i\mathbf{k}' \cdot \mathbf{r}} V(\mathbf{r}) e^{ik_z z} e^{im\phi} \psi(r). \quad (2)$$

Since vortex beams are most easily described in cylindrical coordinates, our first step is to expand the potential in a cylindrical symmetric basis of Bessel functions [32].

$$V(\mathbf{r}) = V(r, \phi, z) \quad (3)$$

$$= \int dk_z'' \int_0^\infty dk_\perp'' k_\perp'' \sum_{m''=-\infty}^\infty V_{m''}(k_\perp'', k_z'') J_{m''}''(k_\perp'' r) e^{im''\phi} e^{ik_z'' z}, \quad (4)$$

with

$$V_{m''}(k_\perp'', k_z'') = \int dz \int_0^\infty dr \int_0^{2\pi} d\phi \times r V(r, \phi, z) J_{m''}(k_\perp'' r) e^{-im''\phi} e^{-ik_z'' z}, \quad (5)$$

the polar expansion coefficients of the potential. Inserting eq. (4) into eq. (2) gives us

$$A_m(\mathbf{k}') = \int d\mathbf{r} \int dk_z'' \int_0^\infty dk_\perp'' k_\perp'' \sum_{m''=-\infty}^\infty V_{m''}(k_\perp'', k_z'') J_{m''}(k_\perp'' r) e^{im''\phi} e^{ik_z'' z} e^{i(k_z - k_z'')z} e^{im\phi} e^{-i\mathbf{k}'_\perp \cdot \mathbf{r}_\perp} \psi(r). \quad (6)$$

This can be simplified using the Jacobi-Anger identity,

$$e^{i\mathbf{k}'_\perp \cdot \mathbf{r}} = e^{ik_\perp r \cos(\phi - \phi_k)} \quad (7)$$

$$= \sum_{m=-\infty}^\infty i^m J_m(k_\perp r) e^{im(\phi - \phi_k)}, \quad (8)$$

to obtain

$$A_m(\mathbf{k}') = \int d\mathbf{r} \int dk_z'' \int_0^\infty dk_\perp'' k_\perp'' \times \sum_{m', m''=-\infty}^\infty (-i)^{m'} V_{m''}(k_\perp'', k_z'') J_{m''}(k_\perp'' r) \times e^{i(m'' + m - m')\phi} e^{i(k_z'' + k_z - k_z'')z} J_{m'}(k'_\perp r) e^{im'\phi_k} \psi(r). \quad (9)$$

Performing the integrals over ϕ and z gives us a Kronecker delta and a Dirac delta function, which finally gives us for the scattering amplitude:

$$A_m(\mathbf{k}') = \int_0^\infty dr r \int dk_z'' \int_0^\infty dk_\perp'' k_\perp'' \sum_{m', m''=-\infty}^\infty (-i)^{m'} V_{m''}(k_\perp'', k_z'') J_{m''}(k_\perp'' r) \delta_{m'' + m - m'} \delta(k_z'' + k_z - k_z'') J_{m'}(k'_\perp r) e^{im'\phi_k} \psi(r) \quad (10)$$

$$= \int_0^\infty dk_\perp'' k_\perp'' \sum_{m'=-\infty}^\infty (-i)^{m'} e^{im'\phi_k} V_{m'-m}(k_\perp'', k_z'' - k_z) \int_0^\infty dr r J_{m'-m}(k_\perp'' r) J_{m'}(k'_\perp r) \psi(r). \quad (11)$$

Eq. (11) is the most general expression to describe vortex scattering in cylindrical coordinates on a potential determined by its polar expansion coefficients $V_{m''}(k_\perp'', k_z'')$.

II. VORTEX SCATTERING ON A HELIX: DERIVATION AND PROPERTIES

A. Derivation

The potential of a helix having pitch P , radius R , with Q point scatterers on one period of the helix, can be

written as

$$V(\mathbf{r}) = \sum_{q,n=-\infty}^{\infty} \delta(r-R) \times \delta\left(\phi - a\frac{2\pi z}{P} + 2\pi n\right) \delta\left(z - \frac{q}{Q}P\right) \quad (12)$$

where $a = +1$ in case of a right-handed helix and $a = -1$ for a left-handed helix. Using eq. (5), we find the potential's expansion coefficients:

$$V_m(k_{\perp}, k_z) = \int dz \int_0^{\infty} dr \int_0^{2\pi} d\phi r J_m(k_{\perp} r) e^{-im\phi} e^{-ik_z z} \times \sum_{q,n=-\infty}^{\infty} \delta(r-R) \delta\left(\phi - a\frac{2\pi z}{P} + 2\pi n\right) \delta\left(z - \frac{q}{Q}P\right). \quad (13)$$

We can rewrite this as

$$V_{m,v}(k_{\perp}) = \frac{1}{P} \int_0^P dz \int_0^{2\pi} d\phi R J_m(k_{\perp} R) e^{-im\phi} e^{-iv\frac{2\pi}{P}z} \sum_{q=1}^Q \delta\left(\phi - a\frac{2\pi z}{P}\right) \delta\left(z - \frac{q}{Q}P\right) = \frac{R}{P} \sum_{q=1}^Q J_m(k_{\perp} R) e^{-i(am+v)\frac{2\pi q}{Q}} \quad (14)$$

$$= \frac{RQ}{P} J_m(k_{\perp} R) \delta\left(\frac{am+v}{Q} - N\right), \quad (15)$$

with $v, N \in \mathbb{Z}$ and $k_z = v\frac{2\pi}{P}$ is quantized because of the periodicity in z .

When dropping the constant $\frac{RQ}{P}$, filling the expansion coefficients (15) into eq. (11) gives us for the scattering amplitude

$$A_m(\mathbf{k}') = \int_0^{\infty} dk'_{\perp} k'_{\perp} \sum_{m'=-\infty}^{\infty} (-i)^{m'} e^{im'\phi_k} \times J_{m'-m}(k'_{\perp} R) \delta\left(\frac{a(m'-m)+v}{Q} - N\right) \times \int_0^{\infty} dr r J_{m'-m}(k'_{\perp} r) J_{m'}(k'_{\perp} r) \psi(r). \quad (16)$$

where the number $v = \frac{P}{2\pi}(k_z - k'_z) \in \mathbb{Z}$ discretizes the transferred forward momentum. The integral over k''_{\perp} is given analytically by

$$\int_0^{\infty} dk'_{\perp} k'_{\perp} J_n(k'_{\perp} r) J_n(k'_{\perp} R) = \frac{\delta(r-R)}{r}, \quad (17)$$

such that we find the final scattering amplitude to be

$$A_m(\mathbf{k}') = \sum_{m'=-\infty}^{\infty} (-i)^{m'} e^{im'\phi_k} \delta\left(\frac{a(m'-m)+v}{Q} - N\right) \int_0^{\infty} dr \delta(r-R) J_{m'}(k'_{\perp} r) \psi(r) \quad (18)$$

$$= e^{i(m-av)\phi_k} \sum_{N=-\infty}^{\infty} (-i)^{aNQ} e^{iaNQ\phi_k} \times J_{m+a(NQ-v)}(k'_{\perp} R) \psi(R) \quad (19)$$

$$= e^{i(m-av)\phi_k} \sum_{N=-\infty}^{\infty} (-i)^{NQ} e^{iNQ\phi_k} \times J_{m-av+NQ}(k'_{\perp} R) \psi(R), \quad (20)$$

where in the last step we replaced the summation over N by one over $-N$ in case of a left-handed helix such that aN is replaced by N for both $a = 1$ and $a = -1$. In what follows we will drop the constant $\psi(R)$.

B. Centrosymmetry when $v = am + nQ, n \in \mathbb{Z}$

When looking at the scattering amplitude for rings for which $v = am + nQ$, or equivalently, $m - av = nQ, n \in \mathbb{Z}$, we get

$$A_m(k'_\perp, \phi_k)|_{m-av=nQ} = e^{inQ\phi_k} \sum_{N=-\infty}^{\infty} (-i)^{NQ} e^{iNQ\phi_k} J_{nQ+NQ}(k'_\perp R) \quad (21)$$

$$= i^{nQ} \sum_{N=-\infty}^{\infty} (-i)^{NQ} e^{iNQ\phi_k} J_{NQ}(k'_\perp R) \quad (22)$$

$$= J_0(k'_\perp R) + \sum_{N=1}^{\infty} ((-i)^{NQ} e^{iNQ\phi_k} J_{NQ}(k'_\perp R) + (-i)^{-NQ} e^{-iNQ\phi_k} J_{-NQ}(k'_\perp R)) \quad (23)$$

$$= J_0(k'_\perp R) + \sum_{N=1}^{\infty} (-i)^{NQ} J_{NQ}(k'_\perp R) (e^{iNQ\phi_k} + e^{-iNQ\phi_k}) \quad (24)$$

$$= J_0(k'_\perp R) + \sum_{N=1}^{\infty} 2(-i)^{NQ} J_{NQ}(k'_\perp R) \cos(NQ\phi_k). \quad (25)$$

Where we omitted a phase factor i^{nQ} . Looking at the scattering amplitude in the point $(k'_\perp, \phi_k + \pi)$, gives us

$$A_m(k'_\perp, \phi_k + \pi)|_{m-av=nQ} = J_0(k'_\perp R) + \sum_{N=1}^{\infty} 2(-i)^{NQ} J_{NQ}(k'_\perp R) \cos(NQ(\phi_k + \pi)) \quad (26)$$

$$= J_0(k'_\perp R) + \sum_{N=1}^{\infty} 2(i)^{NQ} J_{NQ}(k'_\perp R) \cos(NQ(\phi_k)) \quad (27)$$

$$= A_m^*(k'_\perp, \phi_k)|_{m-av=nQ} \quad (28)$$

The intensity of the diffraction pattern, $I(\mathbf{k}')$ is given by the amplitude squared, $|A(\mathbf{k}')|^2$. When we calculate this for the points (k'_\perp, ϕ_k) and $(k'_\perp, \phi_k + \pi)$,

$$I_m(k'_\perp, \phi_k)|_{m-av=nQ} = (A_m(k'_\perp, \phi_k) A_m^*(k'_\perp, \phi_k))|_{m-av=nQ} \quad (29)$$

$$= (A_m^*(k'_\perp, \phi_k + \pi) A_m(k'_\perp, \phi_k + \pi))|_{m-av=nQ} \quad (30)$$

$$= I_m(k'_\perp, \phi_k + \pi)|_{m-av=nQ} \quad (31)$$

we see that these diffraction rings are centrosymmetric.
